Multitracer study with positron emission tomography in Creutzfeldt-Jakob disease

Henry Engler[1, 2], Per Olov Lundberg[2], Karl Ekbom[3], Inger Nennesmo[4], Anna Nilsson[1], Mats Bergström[1], Hideo Tsukada[5], Per Hartvig[1], Bengt Långström[1]

[1] Uppsala University PET Centre, Uppsala University Hospital, SE 751 85 Uppsala, Sweden
[2] Department of Neurology, Uppsala University Hospital, Uppsala, Sweden
[3] Department of Neurology, Huddinge University Hospital, Stockholm, Sweden
[4] Department of Pathology, Huddinge University Hospital, Stockholm, Sweden
[5] Hamamatsu Photonics K.K.Central Research Lab, Hamakita City, Japan

Received: 18 March 2002 / Accepted: 20 August 2002 / Published online: 26 October 2002

Abstract. During the period February 1997 to April 2000, 15 patients with clinical symptoms of Creutzfeldt-Jakob disease (CJD) were referred to Uppsala University PET Centre. Positron emission tomography (PET) was performed to detect characteristic signs of the disease, e.g. neuronal death and/or astrocytosis in the brain. The examinations were performed in one session starting with oxygen-15 labelled water scan to measure regional cerebral blood flow, followed by imaging with the monoamine oxidase B inhibitor *N*-[^{11}C-methyl]-L-deuterodeprenyl (DED) to assess astrocytosis in the brain and finally imaging with fluorine-18 2-fluorodeoxyglucose (FDG) to assess regional cerebral glucose metabolism ($rCMR_{glu}$). Nine of the patients fulfilled the clinical criteria of probable CJD. In eight of them, FDG and DED imaging revealed, in comparison with normal controls, a typical pattern characterized by a pronounced regional decrease (<2SD) in glucose brain metabolism, indicative of neuronal dysfunction; this was accompanied by a similar increase (>2SD) in DED binding, indicating astrocytosis. These changes were most pronounced in the cerebellum and the frontal, occipital and parietal cortices, whereas the pons, the thalamus and the putamen were less affected and the temporal cortex appeared unaffected. The cerebral blood flow showed a pattern similar to that observed with FDG. In the ninth patient, analysis with DED was not possible. The diagnosis of definite CJD according to international consensus criteria was confirmed in six of these patients. In one patient with probable CJD, protease-resistant prion protein (PrPres) could not be demonstrated. In two patients with probable CJD, autopsy was not allowed. Computed tomography and magnetic resonance imaging, performed in four and seven of these nine patients respectively, showed unspecific, mainly atrophic changes. In six other patients, the PET examinations gave a different pattern. In three of them, high $rCMR_{glu}$ was noticed in parts of the brain, particularly in the temporal lobes and basal ganglia, which could suggest encephalitis. One of the patients had Sjögren's syndrome, one had paraneoplastic limbic encephalitis and the third recovered spontaneously. In the other three patients, the DED binding was normal despite a hypometabolic glucose pattern. In conclusion, the PET findings obtained using DED and FDG paralleled neuropathological findings indicating neuronal dysfunction and astrocytosis, changes that are found in CJD.

Keywords: Creutzfeldt-Jakob disease – Positron emission tomography – FDG – Deprenyl – Astrocytosis

Eur J Nucl Med (2003) 30:85–95
DOI 10.1007/s00259-002-1008-x

Henry Engler (✉)
Uppsala University PET Centre,
Uppsala University Hospital, SE 751 85 Uppsala, Sweden
e-mail: henry.engler@pet.uu.se
Tel.: +46-18-6113783, Fax: +46-18-4715390

Introduction

The human forms of the transmissible spongiform encephalopathies (TSE), sporadic Creutzfeldt-Jakob disease (spCJD), familial CJD, fatal familial insomnia, Gerstmann-Sträussler-Scheinker syndrome, variant CJD (vCJD) – related to bovine spongiform encephalopathy (BSE) – and kuru, are all neuropathologically characterized by neuronal loss, astrocytosis, spongiform changes and deposits in the brain of a protease-resistant prion protein (called PrPres or PrPSc). Clinical diagnosis may be difficult since the symptoms are not always specific. Suspicion of the disease may emerge in patients with rapidly progressive dementia and multifocal signs. It is of utmost importance to obtain a diagnosis as early as

possible since some types of rapidly progressive dementia may be associated with treatable diseases (autoimmune, paraneoplastic or viral encephalitis) [1, 2, 3, 4]. The diagnosis of definite CJD is at present only possible through neuropathological examination of brain tissue according to international (WHO and EU) consensus. For ethical, practical and topographic reasons, brain biopsy is not applicable. Computed tomography (CT) scans show only unspecific changes whereas magnetic resonance imaging (MRI) may be of help [5] but is often inconclusive. Periodic sharp wave complexes are found as typical EEG changes in certain genotypes [6]. Laboratory examinations of cerebrospinal fluid for proteins such as 14.3.3 [7] and tau [8] are of importance in the diagnosis of certain types of CJD, e.g. sporadic versus variant type CJD, but may be normal, even in pathologically confirmed cases [9]. CSF analysis of the 14.3.3 protein has been regarded as an important means of assessing the presence of the disease, but was not available at the start of this investigation. So far, no blood assay is available that may help in the diagnosis. There is thus a need for a technique that can illuminate the neuropathological changes in the living patient.

Positron emission tomography (PET) provides a means to use in combination a series of in vivo tracers that can provide information on regional brain metabolism and physiology relevant to the specific pathological changes in brain disorders of the TSE type. Thus, cerebral blood flow can be studied with oxygen-15 labelled water, and changes in glucose metabolism measured by the uptake of fluor-18 2-fluorodeoxyglucose (FDG) may serve as a marker of neuronal dysfunction and death. Furthermore, *N*-[^{11}C-methyl]-L-deuterodeprenyl (DED), a MAO-B inhibitor, has been shown to be a useful marker of astrocytosis/gliosis [10, 11, 12, 13, 14]. Together these three tracers might be of value for the diagnosis of TSE. A technique was developed by which these often seriously ill patients could be examined in the PET scanner, evaluating the influence of sedation – if necessary – on the brain metabolism. The primary goal was to study patients with suspected CJD in order to detect specific patterns of tracer uptake in patients finally proven to have definite CJD or considered to have probable CJD according to international diagnostic criteria. A secondary goal was to try to correlate the regional PET findings with clinical and neuropathological symptoms and signs.

Materials and methods

Patients and healthy control subjects

Fifteen patients aged 60.5±15.5 years (mean and range) with suspected CJD were referred to Uppsala University PET Centre for examination between February 1997 and April 2000. The clinical symptoms and the results of the EEG recordings are given in Table 1. EEG, CT and MRI were performed at the patient's local hospital. Data given in this paper are from original case records. Thus, the original recordings have not been re-examined by us.

Nine subjects (four males and five females) aged 56±8 years (mean age and range) volunteered as normal controls for the examination of regional cerebral glucose metabolic rate ($rCMR_{glu}$). Similarly, another seven subjects (four males and three females) aged 42±13 years (mean age and range) served as a control panel for the assessment of normal DED binding. None of the volunteers had a history of a medical or neurological disease or substance abuse. They were recruited by personal contact or by an advertisement in the local newspaper.

The Ethics Committee at the Uppsala University Medical Faculty and the Radiation Hazard Ethics Committee of Uppsala University Hospital approved the study.

Positron emission tomography

Procedure

Patients and healthy volunteers were examined with radiotracers in the order ^{15}O-H_2O, DED and FDG on the same day after at least a 4-h fasting period before PET. In severely demented patients, it was found necessary to perform PET during propofol anaesthesia. Atropine 0.5 mg was given as premedication and induction was performed with 50±18 mg of propofol (Diprivan, AstraZeneca, UK). Anaesthesia was maintained with 192±52 mg/h propofol for 3.7±0.6 h. Electrocardiography, pulse oxymetry and respiratory rate were measured throughout. Loss of consciousness was defined as unresponsiveness to both verbal and tactile stimuli. Occasionally, assistance in the form of head tilt or jaw thrust before the examination was necessary to maintain a free airway. Supplementary oxygen, 4–8 l/min, was administered via a nose catheter or through a funnel placed in front of the nose and mouth in the case of low blood oxygen saturation.

Radiotracers

^{11}C-DED, ^{18}F-FDG and ^{15}O-H_2O were produced according to the standard operating procedure under GMP rules at the laboratory.

PET scanning

PET was performed in a GE 2048-15B (GE Electronics, USA) brain PET scanner that simultaneously recorded 15 tomographic slices covering an axial field of 10 cm with a slice separation of 6.5 mm and a planar resolution of 5 mm [15]. The central transaxial resolution in scatter medium, applying a 4-mm Hanning filter, was 7.4 mm, measured as the full-width at half-maximum of a Gaussian fit through a profile of a 1-mm inner diameter polyethylene line source in water. The orbitomeatal line was used to centre the subject's head.

A dose of 10 MBq/kg ^{15}O-H_2O was injected intravenously for measurement of regional cerebral blood flow (rCBF), arterial blood radioactivity was measured in discrete samples and the radioactivity in the brain was measured for 17×5 s and 2×20 s.

Patients were administered a rapid bolus of approximately 400 MBq of ^{11}C-DED in a venous catheter in the arm. PET measured the time-dependent uptake of radioactivity in the brain according to a predetermined set of measurements (4×30, 2×60,

1×300 and 4–6×400 s frames) for up to 60 min. Images were reconstructed for each sequential measurement.

Subjects were given 200–300 MBq of ^{18}F-FDG intravenously and the radioactivity in the brain was measured for 5×60, 5×180, 5×300 and 1×600 s frames for 55 min. Arterial blood samples were drawn from the radial artery. The plasma glucose concentration was measured three times, once before and twice after the injection of ^{18}F-FDG.

The scans were corrected for scatter and attenuation using a transmission scan for 10 min and reconstructed with a 6-mm Hanning filter. A computerized re-orientation procedure was used to align consecutive PET studies for accurate intra- and inter-individual comparisons [16].

Regions of interest

All PET investigations were analyzed using identical standardized regions of interest (ROIs) in the brain. The reference slice was that where the thalami were most clearly visible. In this plane both thalami were defined with an area of 1.5 cm^2, and a whole brain ROI was formed at this level. Ventricles were not included. Cortical ROIs with a width of 1 cm and a length of 3 cm were placed in the frontal (three slices) and parietal (four slices) cortices. ROIs for the putamen were placed at the level with the highest uptake. Other cortical ROIs were placed in the anterior cingulate cortex (three slices), the temporo-parietal area (one slice, two slices below the level of the thalamus), the occipital and cerebellar cortices at the level of highest radioactivity uptake and the temporal lobe (five coronal slices). Two ROIs 1.5 cm in diameter were located in the pons and linked, and the white matter was defined with a free-hand ROI at the location of the centrum semiovale. In total, 61 ROIs and 15 volumes of interest (VOIs) were included in the study.

Evaluation

DED. Quantitative estimates of binding to MAO-B and initial tracer distribution were generated by the Patlak method [17], with proposed modifications [18]. The tracer uptake on a pixel-by-pixel basis was divided by the cerebellar cortex tracer concentration and plotted against normalized time, although the cerebellar time-activity data were first multiplied by an exponential. The procedure has been shown to linearize the Patlak graph slope and allows separate generation of images representing the Patlak slope and intercept. This slope has also been found to be proportional to MAO-B enzyme expression [18].

FDG. Parametric maps of glucose metabolic rate were generated by the Patlak technique. Images of glucose metabolic rate were generated with an operational equation derived by Sokoloff [19] and modified by Phelps [20].

In order to reduce inter-subject variability, the values of glucose metabolic rate were normalized to the whole brain to calculate a glucose metabolic index. This standardization ratio of regional glucose metabolic rate allowed direct comparisons of relative metabolism in specific brain regions between subjects. Normalized glucose metabolic rate was used in all regions except the cerebellum. The hypometabolism in the cerebellum and the brain did not keep the same relation in the CJD patients. Changes in the cerebellum that are clearly significant in absolute values may become normal if they are divided by an extremely low whole brain value.

^{15}O-H_2O. A simple two-compartment model was used to determine rCBF [21].

Statistical analysis of PET data

The values for glucose metabolic rate and binding of DED obtained in patients were compared with those in healthy volunteers, and deviations larger than ±2SD were considered significant. For DED, the absolute Patlak slope values in patients were compared directly with those in the healthy subjects.

Asymmetry index

The normalized FDG values and the DED Patlak slope for each of the ROI positions were used in the statistical analysis. For each ROI and tracer the asymmetry index (AI) was calculated as follows:

$$\mathrm{AI} = \mathrm{abs}(\mathrm{ROI}_{dx} - \mathrm{ROI}_{\mathrm{sin}})/(\mathrm{ROI}_{dx} + \mathrm{ROI}_{\mathrm{sin}})/2 \times 100$$

where abs is the absolute value, dx is right and sin is left. These AI values were treated as independent stochastic variables.

The purpose of the statistical analysis was to find whether the AI values and the correlation of these variables differed between groups (nine patients with CJD and the healthy volunteer groups).

The reason for using the AI values rather than the raw data was to minimize the effect of anaesthesia. Anaesthesia produces regional differences in the glucose metabolic rate (frontal, parietal or temporal) but these changes are symmetrical. Consequently, by using the AI values, the effects of anaesthesia were cancelled out.

The Mann-Whitney *U* test was applied adopting the Bonferroni correction to compensate for the problem of mass significance. Accordingly, P values $<0.05/k$, where k=the number of tests, were regarded as significant. Tests of group differences in AI were performed both on the DED slope data set and on the FDG data set. These tests were carried out using Statistica (StatSoft, Inc 1996, Tulsa).

Neuropathology

At autopsy, the brains were fixed in formaldehyde and cut in coronal sections. Gross examination was carried out and numerous representative samples from cerebral cortex, white matter, the basal ganglia, cerebellum and brain stem were collected. Samples from five of the CJD patients (203, 204, 216, 228 and 243) were examined without knowledge of the results of PET. In case 212, tissue blocks from affected regions according to PET were included as well. Blocks were decontaminated for 1 h in concentrated formic acid before paraffin embedding. Five-micrometre-thick sections were cut and stained with haematoxylin-eosin, Luxol fast blue, alkaline Congo red and the modified Bielschowsky's method. Blocks of affected regions were used for PrP (prion protein) immunohistochemistry. Paraffin sections were mounted on silanized slides. The sections were deparaffinated, rinsed for 10 min in concentrated formic acid and treated with microwaves for 3 min with full effect and 15 min with a low effect; thereafter they were incubated for 1 h at room temperature with the monoclonal antibody 3F4 (Senetek, Missouri, USA or DAKO, Glostrup, Denmark). A standard ABC-peroxidase technique was used for detection of immunoreactivity with diaminobenzidine (DAB) as chromogen.

Results

Clinical examination

The results of the neurological examination of the 15 patients are given in Table 1. Nine of the patients fulfilled the clinical criteria of probable CJD when still alive. All CJD patients were severely demented. Aphasia and myoclonus were found in eight of the nine probable CJD patients, and ataxia in seven. The initial symptoms included sensory changes in three patients, anxiety and/or depression in two and dementia in a further two. Other initial signs were apraxia, ataxia or tremor. The age at onset varied from 45.4 to 76.7 years with a mean of 67.3 years. The duration of symptoms varied from 2 to 28 months. Patient 203 had cortical blindness and visual hallucinations and displayed a clinical picture characteristic of the Heidenhain type of CJD [9, 22]. The sensory symptoms consisted of paraesthesias of the right chin (patient 203), paraesthesias of a diffuse nature (patient 212) and changes in taste so that "everything tasted salty" (initial symptom in patient 204).

CT and MRI examinations did not reveal specific changes. EEG recordings showed typical periodic sharp wave complexes in five patients (203, 216, 243, 235, 236), generalized slowing in three patients (207, 212, 228) and unspecific changes in one patient (204).

The other six patients (229, 237, 265, 266, 305, 326) presented with moderate or severe dementia, which was the initial symptom in two of them. Anxiety and/or depression were the initial symptoms in two patients and ataxia in another two. EEG showed non-specific changes in three patients and epileptiform changes in one (patient 326), and was normal in two further patients.

Four patients (229, 237, 266, 305) are still alive after more than 2 years of illness.

In patient 229, MRI revealed high signal in the hippocampus and amygdala on both sides. She improved and is still alive without a diagnosis. Patient 237 is still alive and still demented. CT showed atrophy. Laboratory examination of blood has indicated possible Sjögren's syndrome. The final diagnosis in case 265 was late catatonia. She died after more than 2 years of illness. Neuropathology is pending. In patient 266 frontal lobe dementia was diagnosed clinically. The patient is still alive. Sjögren's syndrome was diagnosed in patient 305. The patient improved after treatment with cytostatic agents. Patient 326 had a small cell pulmonary carcinoma with a paraneoplastic encephalopathy, which was confirmed post mortem.

PET with FDG, DED and H_2O

Tables 2, 3 and 4 respectively summarize the FDG uptake, the DED slope and the DED/FDG ratio for different ROIs..

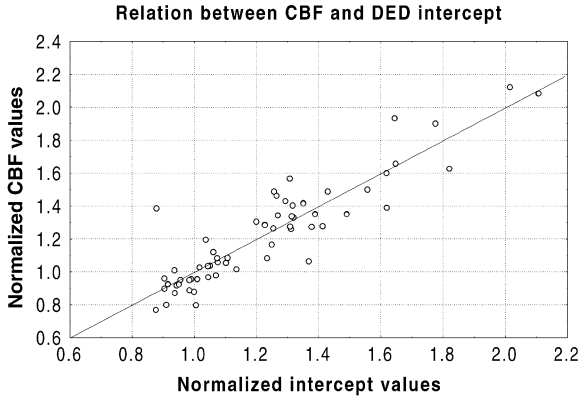

Fig. 1. Normalized CBF and DED intercept values for each region for all CJD patients who were examined with ^{15}O-H_2O (R^2=0.82)

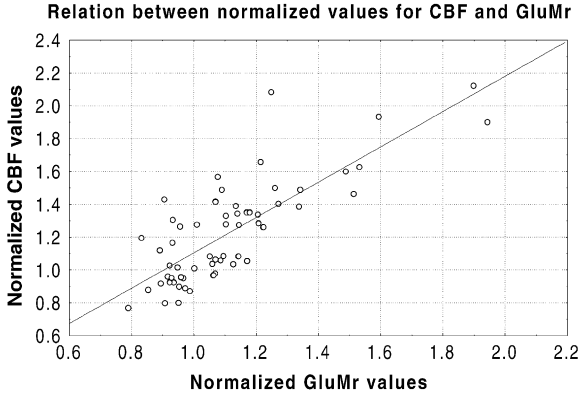

Fig. 2. Normalized CBF and CMR_{glu} values for each region for all CJD patients who had been examined with ^{15}O-H_2O (R^2_{ady}=0.63)

Cerebral blood flow

Comparison of calculated rCBF in ml min^{-1} 100 ml^{-1} and the intercept of the Patlak slope calculated for DED, both normalized against the respective values of the whole brain, revealed a direct relation in all brain regions (Fig. 1). The reduction in the rCBF in patients with neuropathologically confirmed CJD as compared with healthy subjects also followed the decrease in glucose metabolic rate in all ROIs, indicating that glucose hypometabolism and CBF decrease were correlated in different brain regions in the CJD patients (Fig. 2). Therefore, to simplify, rCBF and the DED intercept are not described in this article.

Statistical analysis

Mean plots of the standard deviations from normal

Mean plots were made to obtain a general overview of which areas might be affected in CJD. The values used in the plots were the number of standard deviations that

Table 1. Summary of symptoms in 15 patients referred with suspected CJD

Patient	Sex	Onset	Age at death	Dementia	Anxiety, depression	Aphasia	Apraxia	Ataxia	Myoclonus	Rigidity	Tremor	Chorea	Akinetic mutism	Pyramidal symptoms	Cranial nerves	Sensory	Halluci-nations	Focal	Incontinens	EEG
Definite CJD																				
203	M	45 3/12	45 5/12	+	+	+		+	+	+	+	+	+		+	X	+			Typ
204	F	72 0/12	72 6/12	+	+	+		+								X	+			Nspec
212	F	52 8/12	55 0/12	+	X	+	+	+	+	+		+		+		X				Slow
216	F	70 7/12	71 2/12	+			X		+			+	+	+						Typ
228	F	60 0/12	60 6/12	+		+		X	+	+	+	+						+	+	Slow
243	F	54 9/12	56 2/12	X		+	+		+	+	+			+						Typ
Probable CJD																				
235	F	54 6/12	54 9/12	X		+	+	+	+	+									+	Typ
236	F	76 8/12	77 0/12	+	X	+		+	+								+	+		Typ
Clinically probable CJD. Not PAD verified																				
207	M	75 7/12	75 10/12	+		+	+	+	+		X									Slow
Non-CJD																				
229	F	68 4/12	A>4 years	+		+	+	X			+			+			+	+		Norm
237	F	68 9/12	A>4 years	X	+				+	+							X	+		Nspec
265	F	70 0/12	72 x/12	+	X	+					+		+							Norm
266	F	63 7/12	A >3 years	+				X						+						Nspec
305	F	52 5/12	A>2 years	+	X													+		Nspec
326	F	63 9/12	64 9/12	X													+	+		Epilep

+, Symptom present during course of illness; X, initial symptom; A>*n* years, still alive after *n* years; EEG, last investigation of a series; PAD, patho-anatomical diagnosis; Typ, typical; Nspec, non-specific

Table 2. FDG uptake: standard deviations compared with controls

Region	Definite CJD												Probable CJD								Total
	Pat. 203		Pat. 204		Pat. 212		Pat. 216		Pat. 228		Pat. 243		Pat. 235		Pat. 236						
	R	L	R	L	R	L	R	L	R	L	R	L	R	L	R	L					
Pons																					0
CBL ctx	–4 SD	–4 SD	–4 SD	–4 SD	–3 SD	–3 SD	–4 SD	–4 SD	–4 SD	–4 SD	–5 SD	–5 SD	–4 SD	–4 SD	–5 SD	–5 SD					8
CBR WhM																					0
Cing ant			–2 SD	–3 SD			–4 SD	–2 SD	–3 SD	–6 SD			–3 SD		–2 SD						5
Fr ctx 1[a]	–2 SD		–2 SD	–6 SD		–4 SD	–5 SD	–2 SD	–3 SD	–4 SD	–4 SD	–4 SD	–4 SD		–3 SD	–5 SD					8
Fr ctx 2[a]			–2 SD	–4 SD		–3 SD	–3 SD	–2 SD	–2 SD	–2 SD	–3 SD	–2 SD	–3 SD		–2 SD	–2 SD					7
Frass ctx	–2 SD	–2 SD	–2 SD	–5 SD		–4 SD	–3 SD		–4 SD	–3 SD	–2 SD	–3 SD	–4 SD		–3 SD	–4 SD					8
Par ctx 1[a]		–2 SD		–2 SD		–3 SD	–3 SD				–3 SD	–3 SD	–2 SD			–2 SD					6
Par ctx 2[a]	–3 SD			–3 SD		–4 SD	–4 SD		–2 SD		–5 SD	–2 SD	–3 SD		–3 SD	–5 SD					8
Par ctx 3[a]	–3 SD			–3 SD		–3 SD	–3 SD				–4 SD	–2 SD	–3 SD		–2 SD	–3 SD					7
Par ctx 4[a]	–2 SD	–3 SD	–2 SD	–5 SD		–3 SD	–3 SD		–2 SD		–5 SD	–3 SD	–4 SD			–4 SD					8
ParTmp ctx	–3 SD				–3 SD	–4 SD	–2 SD				–3 SD	–3 SD	–3 SD								5
Occipital ctx	–3 SD	–3 SD	–2 SD	–2 SD			–3 SD	–2 SD	–2 SD		–2 SD				–2 SD	–2 SD					6
Putamen									–2 SD	–2 SD						–3 SD					2
SM ctx							–2 SD						–3 SD								2
Thalamus	–4 SD	–2 SD								–3 SD			–2 SD			–3 SD					4
Tmp inf ant																					0
Tmp inf post																					0
Tmp lat ant				–3 SD																	0
Tmp lat post	–3 SD			–2 SD		–5 SD					–2 SD		–2 SD								5
Uncus ant																					0
Uncus post																					0

CBL, cerebellum; CRB WhM, cerebral white matter; Cing, cingulum; Fr ctx, frontal cortex; Frass ctx, frontal association cortex; Par ctx, parietal cortex; ParTmp ctx, parietotemporal cortex; SM, sensorimotor cortex; Tmp, temporal; ant, anterior; inf, inferior; lat, lateral; R, right; L, left; SD, standard deviations; [a]1–4, number of slices above the level of thalami

Table 3. DED slope: standard deviations compared with controls

Region	Definite CJD										Probable CJD				Total
	Pat. 203		Pat. 204		Pat. 216		Pat. 228		Pat. 243		Pat. 235		Pat. 236		
	R	L	R	L	R	L	R	L	R	L	R	L	R	L	
Pons															0
CBL ctx	+4 SD	+5 SD	+4 SD	+4 SD			+4 SD	+7 SD	+6 SD	+7 SD		+2 SD		+3 SD	6
CBR WhM	+3 SD	+3 SD		+4 SD	+4 SD	+3 SD	+4 SD	+5 SD	+6 SD	+7 SD	+2 SD	+2 SD	+3 SD	+4 SD	7
Cing ant															0
Fr ctx 1[a]	+2 SD				+4 SD	+4 SD	+2 SD			+3 SD	+3 SD				5
Fr ctx 2[a]	+2 SD				+3 SD	+3 SD	+2 SD			+2 SD	+3 SD			+2 SD	6
Frass ctx	+3 SD	+3 SD		+3 SD	+5 SD	+4 SD	+4 SD	+4 SD		+2 SD				+4 SD	6
Par ctx 1[a]	+3 SD	+3 SD			+3 SD	+5 SD		+2 SD							3
Par ctx 2[a]	+9 SD	+5 SD			+8 SD	+5 SD	+5 SD	+5 SD		+6 SD	+2 SD				5
Par ctx 3[a]	+3 SD	+3 SD			+4 SD	+3 SD	+4 SD			+7 SD					4
Par ctx 4[a]	+3 SD	+3 SD			+5 SD	+3 SD		+2 SD		+6 SD					4
ParTmp ctx		+2 SD			+3 SD	+3 SD				+4 SD					3
Occipital ctx	+11 SD	+12 SD	+4 SD	+5 SD	+3 SD	+4 SD	+2 SD	+4 SD			+3 SD				5
Putamen					+2 SD	+3 SD	+3 SD	+4 SD							2
SM ctx		+2 SD						+2 SD							2
Thalamus	+4 SD						+5 SD	+4 SD							2
Tmp inf ant															0
Tmp inf post															0
Tmp lat ant															0
Tmp lat post					+3 SD										1
Uncus ant													+2 SD		1
Uncus post					+4 SD	+4 SD	+2 SD	+2 SD							2

CBL, cerebellum; CRB WhM, cerebral white matter; Cing, cingulum; Fr ctx, frontal cortex; Frass ctx, frontal association cortex; Par ctx, parietal cortex; ParTmp ctx, parietotemporal cortex; SM, sensorimotor cortex; Tmp, temporal; ant, anterior; inf, inferior; lat, lateral; R, right; L, left; SD, standard deviations; [a]1–4, number of slices above the level of thalami

Table 4. Brain regions with a significantly increased DED/FDG ratio

Region	Definite CJD										Probable CJD				Total
	Pat. 203		Pat. 204		Pat. 216		Pat. 228		Pat. 243		Pat. 235		Pat. 236		
	R	L	R	L	R	L	R	L	R	L	R	L	R	L	
Pons															0
CBL ctx	+	+	+	+			+	+	+	+		+		+	6
CBR WhM															0
Cing ant															0
Fr ctx 1[a]	+				+	+	+			+	+				4
Fr ctx 2[a]					+	+	+			+	+			+	5
Frass ctx	+	+		+	+		+	+		+				+	6
Par ctx 1[a]		+			+										2
Par ctx 2[a]	+				+		+			+	+				5
Par ctx 3[a]	+				+					+					3
Par ctx 4[a]	+	+			+					+					3
ParTmp ctx					+					+					2
Occipital ctx	+	+	+	+	+	+	+								4
Putamen							+	+							1
SM ctx															0
Thalamus	+							+							2
Tmp inf ant															0
Tmp inf post															0
Tmp lat ant															0
Tmp lat post															0
Uncus ant															0
Uncus post															0

CBL, cerebellum; CRB WhM, cerebral white matter; Cing, cingulum; Fr ctx, frontal cortex; Frass ctx, frontal association cortex; Par ctx, parietal cortex; ParTmp ctx, parietotemporal cortex; SM, sensorimotor cortex; Tmp, temporal; ant, anterior; inf, inferior; lat, lateral; R, right; L, left; SD, standard deviations; [a]1–4, number of slices above the level of thalami

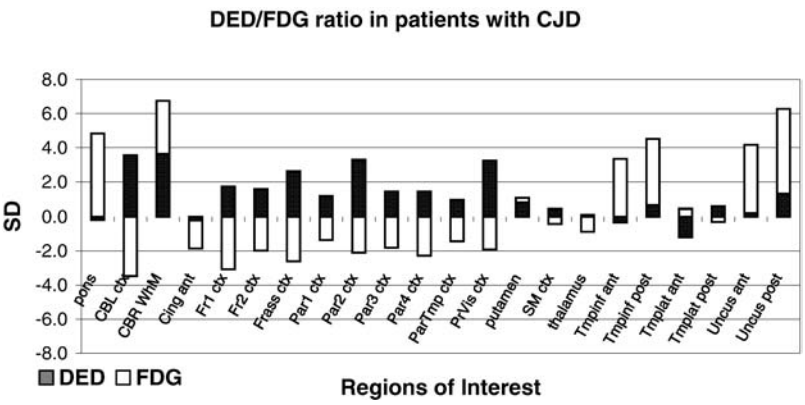

Fig. 3. Bar graph showing the mean change from normal (in standard deviations) for each ROI in patients with CJD. *Ant*, anterior; *inf*, inferior; *post*, posterior; *ctx*, cortex; *CBL*, cerebellum; *CBR WhM*, cerebral white matter; *Cing*, cingulum; *Fr*, frontal; *Frass*, frontal association; *Par*, parietal; *ParTmp*, parietotemporal; *PrVis*, primary visual; *SM*, sensorimotor; *Th*, thalamus; *tmp*, temporal

the DED slope/normalized FDG values for each patient and each ROI differed from the normal group, i.e.:

$$\text{No.SD} = \text{ROI}_{\text{CJD}} - \text{ROI}_{\text{NORM MEAN}} / \text{ROI}_{\text{NORM SD}}$$

The FDG values for each region were divided by the value of the whole brain to reduce the effect of anaesthesia, i.e. all FDG values with the exception of those from the cerebellum are relative to the whole brain.

Areas with a high DED/FDG ratio were found in eight of the nine patients with probable CJD (Fig. 3).

Tests of group difference

Reported *P* values were not corrected for multiple comparisons. The Bonferroni correction for 22 different comparisons was used (alpha =0.05/22).

FDG. Low *P* values for some ROIs were detected, for example the cerebellum (*P*=0.005), the inferior part (*P*=0.013) and apical level (*P*=0.010) of the parietal lobes, the sensorimotor cortex (*P*=0.018) and three ROIs in the temporal lobe [inferior temporal posterior (*P*=0.025), lateral temporal anterior (*P*=0.007) and lateral temporal posterior (*P*=0.013)]. However, when applying the Bonferroni correction for 22 independent tests, none of the results were significant at the 5% level. To obtain a more sensitive test, the sum of all ROI AIs for each subject were calculated and tested for differences between groups. This yielded a *P* value of 0.002, and this result even passed the Bonferroni correction.

DED slope. The test for difference in AI for the thalamus between the CJD group and the healthy volunteer group showed a *P* value of 0.037. This was far from significant when the Bonferroni correction for 22 independent samples was applied. The other test results all had higher *P* values. The more sensitive test of the sum of AIs had a *P* value of 0.010, which was not significant using the Bonferroni correction.

Neuropathological and PET findings

Seven of the nine patients who fulfilled the WHO/EU criteria of probable CJD (WHO 1996) were available for neuropathological examination of the brain. Six of them were found to have definite CJD. In a seventh patient who fulfilled the clinical criteria for CJD, PrPres could not be demonstrated. The brain of this patient showed mild astrocytosis and moderate neuronal loss but definitive diagnosis was not made. In two patients, autopsy was not performed. Examination of the brain in the seven patients revealed cortical atrophy of varying degrees, particularly in the neocortex (5/7) and cerebellar and temporal cortices, as well as ventricular enlargement in some cases. Microscopy showed pronounced spongiform changes in cortical areas and basal ganglia in all the patients, whereas astrogliosis and neuronal loss were evident in six patients. Immunoreactive products for PrPres deposits were found in six patients.

Eight of the nine patients with probable CJD showed a high DED/FDG ratio consisting in a regional pronounced decrease (<2SD) in glucose brain metabolism that was indicative of neuronal dysfunction, and a similar increase (>2SD) in DED binding, indicating astrocytosis. A high DED/FDG ratio was also found in the patient with negative PrPres. DED examination was not performed in the ninth patient.

The six patients in whom the diagnosis of CJD could not be confirmed showed another pattern of radiotracer distribution. Three of the patients (305, 229, 326) had a regional increase in $rCMR_{glu}$ that was suggestive of encephalopathy, for example of autoimmune, viral or paraneoplastic origin [23]. In these patients, glucose hypermetabolism was obvious particularly in the temporal lobe and also in the striatum, insula and anterior cingulate cortex – a finding that we have not so far seen in CJD. In patient 305, the diagnosis of Sjögren's syndrome was confirmed at biopsy. In patient 229, no aetiology was found but a viral infection or a para-infectious manifestation was suspected. In patient 326, autopsy revealed a paraneoplastic limbic encephalitis. The other three patients showed a diffuse hypometabolism

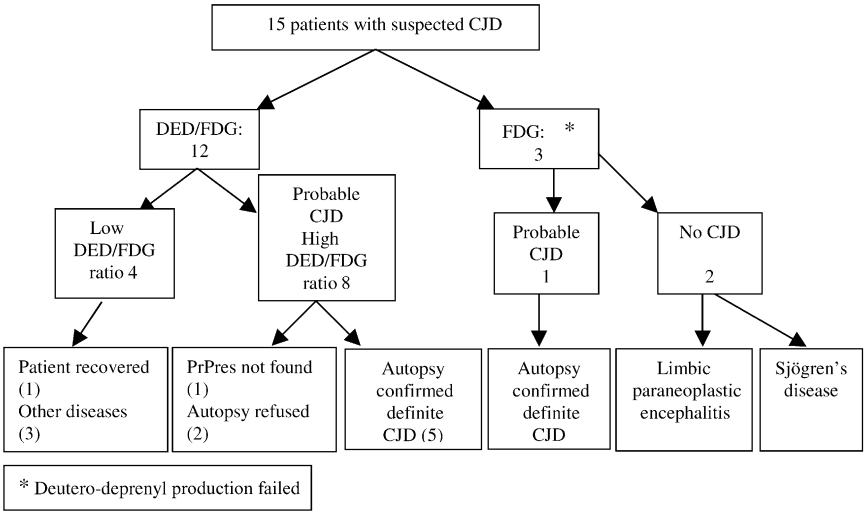

Fig. 4. PET examinations and results in 15 patients referred to the Uppsala PET Centre with suspected CJD

with normal deprenyl uptake, giving a low DED/FDG ratio (Fig. 4).

Discussion

The effect of anaesthesia

Previous studies with FDG have shown heterogeneous, reduced metabolism throughout the brain in patients with CJD. Asymmetry in the distribution of the hypometabolic regions has been found, and frontal, parietal and temporal reduction in glucose uptake has been described [24, 25, 26]. However, in order to perform the PET examinations, anaesthesia was necessary in these severely demented patients, which raised the question of the effects of propofol administration on $rCMR_{glu}$ and DED binding. Previously, propofol anaesthesia titrated to a point just passing the loss of responsiveness in humans was found to be associated with a 55% reduction in whole brain $rCMR_{glu}$ together with regional metabolic alterations [27]. On the other hand, a study by Vandesteene et al. [28] could not find any significant changes in global glucose metabolism in humans during propofol anaesthesia. In the baboon an 18%–36% reduction in whole brain glucose metabolism was, however, shown [29]. Because of these contradictory results, a pilot study using rhesus monkeys in awake and sedated states was performed to evaluate the propofol-induced changes (Fig. 5). No significant effect of propofol anaesthesia on DED binding was seen, whereas there were pronounced dose-dependent decreases in $rCMR_{glu}$ without symmetrical differences.

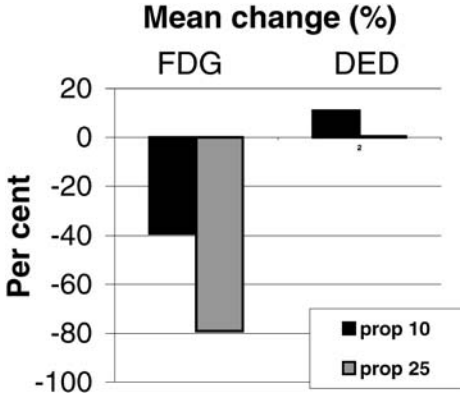

Fig. 5. Effect of propofol anaesthesia on CMR_{glu} and binding of DED to MAO-B in the brain of rhesus monkey (n=3). Monkeys were maintained and handled in accordance with recommendations of the US National Institutes of Health and the guidelines of the Central Research laboratory, Hamamatsu Photonics. Studies were done in the awake stereotactically positioned monkey (for study conditions see [33] and following anaesthesia with propofol. Anaesthesia was given with an intravenous induction dose of 5 mg/kg and maintained with 10 or 25 mg/kg per hour throughout scanning. PET was performed using a high-resolution SHR-7000 PET camera system (Hamamatsu Photonics KK, Japan) with a 2.6-mm full-width at half-maximum [34]. Propofol anaesthesia did not have any significant effect on DED binding, while there was an obvious dose-dependent decrease in CMR_{glu}, the mean reductions being 38%±13% at 10 mg/kg per hour and 77%±5% at 25 mg/kg per hour. During anaesthesia with 10 mg/kg propofol per hour, the decrease varied by 6% (occipital lobe) to 57% (temporal lobe), whereas it varied by 65% (cerebellum) to 85% (striatum) with the dose of 25 mg/kg per hour

One patient with a final diagnosis of definite CJD (212) was examined without anaesthesia and the pattern of glucose uptake was similar to that found in the patients with CJD who were examined under anaesthesia. This argues for a pattern of glucose uptake that persists in spite of the anaesthesia, rather than being caused by it. One of the patients who did not fulfill the criteria for CJD (229) showed hypermetabolic activity in particular areas of the brain, a phenomenon that was not seen in patients with definite or probable CJD. This means that hypermetabolism may be present in spite of anaesthesia.

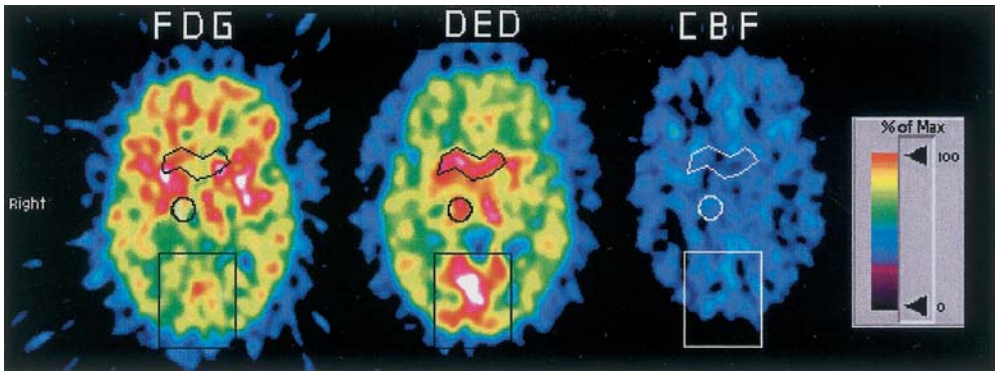

Fig. 6. Patient 203: Heidenhain type of CJD. Areas with high DED binding and low CMR_{glu} are indicated. The cerebral blood flow is very low in the area of nuclei caudati. The occipital area and the right thalamus show less decrease in blood flow

The DED/FDG tracer combination

Results obtained with the combination of DED (as an indicator of gliosis in affected parts of the brain, as reflected by increased DED binding) and FDG (to measure the reduction in the glucose metabolic rate, indicating neuronal dysfunction) showed a strong correlation with the neuropathological changes of astrocytosis and neuronal death in five of the six patients examined. In one patient it was not possible to obtain the DED slope values. The pattern of FDG uptake in this patient was different from that seen in patients with Alzheimer's disease or frontotemporal dementia. Neuropathological examination confirmed CJD. A high DED/FDG ratio was also found in the two other patients with probable CJD and in the patient with negative PrPres at autopsy. The regions that showed a high ratio were the cerebellum and the frontal, occipital and parietal cortices. Central structures such as the putamen and the thalamus were less affected. A high ratio was not found in the temporal lobes, the pons, the cingulum anterior or the sensorimotor cortex of the patients with definite or probable CJD. The regional distribution of the DED/FDG changes was clearly asymmetrical left to right in all eight patients. This was in accordance with the neuropathological findings. However, for obvious reasons it was difficult to compare the particular PET ROI with the limited parts of the cerebral cortex that could be examined by the neuropathologist. In the patient (case 203) with the Heidenhain subtype of spCJD, very strong correlations were found between the clinical symptoms and signs of cortical blindness and visual hallucinations, the profound neuropathological changes in the occipital cortex and the very high DED uptake (>11 SD) in the occipital ROI bilaterally (Fig. 6). In the remaining six patients, it was very difficult to compare the DED/FDG findings with the clinical picture and also to find a correlation.

An age-related increase in DED binding, which was smaller than the level of DED binding reported in postmortem studies, has been described [30]. Obviously the magnitude of the changes that we found considerably exceeds that of the changes caused by the age difference between patients and control subjects.

It has been reported in the literature that patients with spCJD often show high signal intensity on T2-weighted or FLAIR MRI images in the basal ganglia and the putamen in particular [31]. Another very interesting finding is that patients with vCJD related to bovine spongiform encephalopathy show high signal intensity in the pulvinar thalami [32]. Among our patients, the characteristic DED/FDG pattern was seen in the putamen in only one patient (228) and in the thalamus in two patients (203 and 228). Nor did the decrease in FDG uptake or the DED slope show any consistent findings as regards the basal ganglia. Thus, this PET study cannot help to explain the reported MRI findings.

In the six patients in whom suspected CJD was not confirmed, a different pattern of tracer distribution was observed. Three of these patients showed hypermetabolism in the temporal lobes and the basal ganglia. In the patients with CJD, the temporal lobes were the less affected part of the brain.

In the remaining three patients, the pattern of glucose uptake was similar to that found in the patients with CJD, but the DED binding was normal.

Conclusion

Patients with definite or probable CJD showed a typical pattern characterized by simultaneously high DED binding and low FDG uptake, affecting particular regions of the brain and cerebellum but not the temporal lobes (Table 4). The other patients examined showed a different pattern characterized by hypermetabolism particularly in the temporal lobes or a low DED/FDG ratio. The PET findings using DED and FDG paralleled the neuropathological findings indicating neuronal dysfunction and astrocytosis, changes that are found in CJD.

Acknowledgements. The financial support provided by the Uppsala County Council is gratefully acknowledged.

We wish to thank Sven Valind, Johan Valtyson, Jens Sörensen, Eva-Lise Lundberg, Rita Öhrstedt, Carin Lidström, Lars Martin Lindsjö, Mark Lubberink, Robert Moulder, Karl Johan Fasth, Margareta Björkman, Mathias Ögren, Gunnar Antoni, Anna Bergman, Harald Schneider and Joakim Schultz for their excellent technical assistance.

References

1. Meyer MA, Hubner KF, Raja S, Hunter K, Paulsen WA. Sequential positron emission tomographic evaluations of brain metabolism in acute herpes encephalitis. *J Neuroimaging* 1994; 4:104–105.
2. Provenzale JM, Barboriak DP, Coleman RE. Limbic encephalitis: comparison of FDG PET and MR imaging findings. *AJR Am J Roentgenol* 1998; 170:1659–1660.
3. Weiner SM, Otte A, Schumacher M, et al. Alterations of cerebral glucose metabolism indicate progress to severe morphological brain lesions in neuropsychiatric systemic lupus erythematosus. *Lupus* 2000; 9:386–389.
4. Gultekin SH, Rosenfeld MR, Voltz R, Eichen J, Posner JB, Dalmau J. Paraneoplastic limbic encephalitis: neurological symptoms, immunological findings and tumour association in 50 patients. *Brain* 2000; 123:1481–1494.
5. Matoba M, Tonami H, Miyaji H, Yokota H, Yamamoto I. Creutzfeldt-Jakob disease: serial changes on diffusion-weighted MRI. *J Comput Assist Tomogr* 2001; 25:274–277.
6. Parchi P, Giese A, Capellari S, et al. Classification of sporadic Creutzfeldt-Jakob disease based on molecular and phenotypic analysis of 300 subjects. *Ann Neurol* 1999; 46:224–233.
7. Zerr I, Pocchiari M, Collins S, et al. Analysis of EEG and CSF 14-3-3 proteins as aids to the diagnosis of Creutzfeldt-Jakob disease. *Neurology* 2000; 55:811–815.
8. Green AJ, Thompson EJ, Stewart GE, et al. Use of 14-3-3 and other brain-specific proteins in CSF in the diagnosis of variant Creutzfeldt-Jakob disease. *J Neurol Neurosurg Psychiatry* 2001; 70:744–748.
9. Jacobs DA, Lesser RL, Mourelatos Z, Galetta SL, Balcer LJ. The Heidenhain variant of Creutzfeldt-Jakob disease: clinical, pathologic, and neuroimaging findings. *J Neuroophthalmol* 2001; 21:99–102.
10. Stenstrom A, Arai Y, Oreland L. Intra- and extraneuronal monoamineoxidase-A and -B activities after central axotomy (hemisection) on rats. *J Neural Transm* 1985; 61:105–113.
11. Nakamura S, Kawamata T, Akiguchi I, Kameyama M, Nakamura N, Kimura H. Expression of monoamine oxidase B activity in astrocytes of senile plaques. *Acta Neuropathol* 1990; 80:419–425.
12. Ekblom J, Jossan SS, Bergstrom M, Oreland L, Walum E, Aquilonius SM. Monoamine oxidase-B in astrocytes. *Glia* 1993; 8:122–132.
13. Jossan SS, d'Argy R, Gillberg PG, et al. Localization of monoamine oxidase B in human brain by autoradiographical use of ^{11}C-labelled L-deprenyl. *J Neural Transm* 1989; 77:55–64.
14. Jossan SS, Gillberg PG, d'Argy R, et al. Quantitative localization of human brain monoamine oxidase B by large section autoradiography using L-[^{3}H]deprenyl. *Brain Res* 1991; 547:69–76.
15. Holte S, Eriksson L, Dahlbom M. A preliminary evaluation of the Scanditronix PC2048-15B brain scanner. *Eur J Nucl Med* 1989; 15:719–721.
16. Andersson JL, Thurfjell L. Implementation and validation of a fully automatic system for intra- and interindividual registration of PET brain scans. *J Comput Assist Tomogr* 1997; 21:136–144.
17. Patlak CS, Blasberg RG, Fenstermacher JD. Graphical evaluation of blood-to-brain transfer constants from multiple-time uptake data. *J Cereb Blood Flow Metab* 1983; 3:1–7.
18. Bergstrom M, Kumlien E, Lilja A, Tyrefors N, Westerberg G, Langstrom B. Temporal lobe epilepsy visualized with PET with ^{11}C-L-deuterium-deprenyl – analysis of kinetic data. *Acta Neurol Scand* 1998; 98:224–231.
19. Sokoloff L, Reivich M, Kennedy C, et al. The [^{14}C]deoxyglucose method for the measurement of local cerebral glucose utilization: theory, procedure, and normal values in the conscious and anesthetized albino rat. *J Neurochem* 1977; 28:897–916.
20. Phelps ME, Huang SC, Hoffman EJ, Selin C, Sokoloff L, Kuhl DE. Tomographic measurement of local cerebral glucose metabolic rate in humans with (F-18)2-fluoro-2-deoxy-D-glucose: validation of method. *Ann Neurol* 1979; 6:371–388.
21. Raichle ME, Martin WR, Herscovitch P, Mintun MA, Markham J. Brain blood flow measured with intravenous $H_2(^{15})O$. II. Implementation and validation. *J Nucl Med* 1983; 24:790–798.
22. Mathews D, Unwin DH. Quantitative cerebral blood flow imaging in a patient with the Heidenhain variant of Creutzfeldt-Jakob disease. *Clin Nucl Med* 2001; 26:770–773.
23. Fakhoury T, Abou-Khalil B, Kessler RM. Limbic encephalitis and hyperactive foci on PET scan. *Seizure* 1999; 8:427–431.
24. Friedland RP, Prusiner SB, Jagust WJ, Budinger TF, Davis RL. Bitemporal hypometabolism in Creutzfeldt-Jakob disease measured by positron emission tomography with [^{18}F]-2-fluorodeoxyglucose. *J Comput Assist Tomogr* 1984; 8:978–981.
25. Goldman S, Laird A, Flament-Durand J, et al. Positron emission tomography and histopathology in Creutzfeldt-Jakob disease. *Neurology* 1993; 43:1828–1830.
26. Matochik JA, Molchan SE, Zametkin AJ, Warden DL, Sunderland T, Cohen RM. Regional cerebral glucose metabolism in autopsy-confirmed Creutzfeldt-Jakob disease. *Acta Neurol Scand* 1995; 91:153–157.
27. Alkire MT, Haier RJ, Barker SJ, Shah NK, Wu JC, Kao YJ. Cerebral metabolism during propofol anesthesia in humans studied with positron emission tomography. *Anesthesiology* 1995; 82:393–403; discussion 327A.
28. Vandesteene A, Trempont V, Engelman E, et al. Effect of propofol on cerebral blood flow and metabolism in man. *Anaesthesia* 1988; 43 Suppl:42–43.
29. Van Hemelrijck J, Fitch W, Mattheussen M, Van Aken H, Plets C, Lauwers T. Effect of propofol on cerebral circulation and autoregulation in the baboon. *Anesth Analg* 1990; 71: 49–54.
30. Fowler JS, Volkow ND, Wang GJ, Logan J, Pappas N, Shea C, MacGregor R. Age related increases in brain monoamine oxidase B in living healthy subjects. *Neurobiol Aging* 1997; 4:431–435.
31. Collie DA, Sellar RJ, Zeidler M, Colchester AC, Knight R, Will RG. MRI of Creutzfeldt-Jakob disease: imaging features and recommended MRI protocol. *Clin Radiol* 2001; 56: 726–739.
32. Molloy S, O'Laoide R, Brett F, Farrell M. The "Pulvinar" sign in variant Creutzfeldt-Jakob disease. *AJR Am J Roentgenol* 2000; 175:555–556.
33. Onoe H, Inoue O, Suzuki K, et al. Ketamine increases the striatal *N*-[^{11}C]methylspiperone binding in vivo: positron emission tomography study using conscious rhesus monkey. *Brain Res* 1994; 663:191–198.
34. Tsukada H, Harada N, Nishiyama S, Ohba H, Kakiuchi T. Cholinergic neuronal modulation alters dopamine D_2 receptor availability in vivo by regulating receptor affinity induced by facilitated synaptic dopamine turnover: positron emission tomography studies with microdialysis in the conscious monkey brain. *J Neurosci* 2000; 20:7067–7073.